β-delayed neutron spectroscopy of ^{133}In

Z. Y. Xu,[1] M. Madurga,[1] R. Grzywacz,[1,2] T. T. King,[1,2] A. Algora,[3,4] A. N. Andreyev,[5,6] J. Benito,[7,8,9] T. Berry,[10] M. J. G. Borge,[11] C. Costache,[12] H. De Witte,[13] A. Fijalkowska,[14,15] L. M. Fraile,[7] H. O. U. Fynbo,[16] A. Gottardo,[17] C. Halverson,[1] L. J. Harkness-Brennan,[18] J. Heideman,[1] M. Huyse,[13] A. Illana,[13,19] Ł. Janiak,[15,20] D. S. Judson,[18] A. Korgul,[15] T. Kurtukian-Nieto,[21] I. Lazarus,[22] R. Lică,[23,12] R. Lozeva,[24] N. Marginean,[12] R. Marginean,[12] C. Mazzocchi,[15] C. Mihai,[12] R. E. Mihai,[12] A. I. Morales,[3] R. D. Page,[18] J. Pakarinen,[19,25] M. Piersa-Siłkowska,[15] Zs. Podolyák,[10] P. Sarriguren,[11] M. Singh,[1] Ch. Sotty,[12] M. Stepaniuk,[15] O. Tengblad,[11] A. Turturica,[12] P. Van Duppen,[13] V. Vedia,[7] S. Viñals,[11] N. Warr,[26] R. Yokoyama,[1] and C. X. Yuan[27]

[1]*Department of Physics and Astronomy, University of Tennessee, Knoxville, Tennessee 37996, USA*
[2]*Physics Division, Oak Ridge National Laboratory, Oak Ridge, Tennessee 37831, USA*
[3]*Instituto de Física Corpuscular, CSIC-Universidad de Valencia, E-46071, Valencia, Spain*
[4]*Institute for Nuclear Research (ATOMKI), H-4026 Debrecen, Bem ter 18/c, Hungary*
[5]*School of Physics, Engineering and Technology, University of York, North Yorkshire YO10, 5DD, United Kingdom*
[6]*Advanced Science Research Center, Japan Atomic Energy Agency, Tokai-mura, Japan*
[7]*Grupo de Física Nuclear and IPARCOS, Facultad de CC. Físicas, Universidad Complutense de Madrid, E-28040 Madrid, Spain*
[8]*Istituto Nazionale di Fisica Nucleare, Sezione di Padova, I-35131, Padova, Italy*
[9]*Dipartimento di Fisica e Astronomia, Universitá di Padova, I-35131 Padova, Italy*
[10]*Department of Physics, University of Surrey, Guildford GU2 7XH, United Kingdom*
[11]*Instituto de Estructura de la Materia, IEM-CSIC, Serrano 113 bis, E-28006 Madrid, Spain*
[12]*Horia Hulubei National Institute for Physics and Nuclear Engineering, RO-077125 Bucharest, Romania*
[13]*KU Leuven, Instituut voor Kern- en Stralingsfysica, B-3001 Leuven, Belgium*
[14]*Department of Physics and Astronomy, Rutgers University, New Brunswick, New Jersey 08903, USA*
[15]*Faculty of Physics, University of Warsaw, PL 02-093 Warsaw, Poland*
[16]*Department of Physics and Astronomy, Aarhus University, DK-8000 Aarhus C, Denmark*
[17]*IPN, IN2P3-CNRS, Université Paris-Sud, Université Paris Saclay, 91406 Orsay Cedex, France*
[18]*Department of Physics, Oliver Lodge Laboratory, University of Liverpool, Liverpool L69 7ZE, United Kingdom*
[19]*University of Jyväskylä, Department of Physics, P.O. Box 35, FI-40014, Jyväskylä, Finland*
[20]*National Centre for Nuclear Research, 05-400 Otwock, świerk, Poland*
[21]*CENBG, Université de Bordeaux—UMR 5797 CNRS/IN2P3, Chemin du Solarium, 33175 Gradignan, France*
[22]*STFC Daresbury, Daresbury, Warrington WA4 4AD, United Kingdom*
[23]*ISOLDE, EP Department, CERN, CH-1211 Geneva, Switzerland*
[24]*Université Paris-Saclay, IJCLab, CNRS/IN2P3, F-91405 Orsay, France*
[25]*Helsinki Institute of Physics, University of Helsinki, P.O. Box 64, FIN-00014, Helsinki, Finland*
[26]*Institut für Kernphysik, Universität zu Köln, 50937 Köln, Germany*
[27]*Sino-French Institute of Nuclear Engineering and Technology, Sun Yat-Sen University, Zhuhai, 519082, Guangdong, China*

(Received 2 December 2022; accepted 13 June 2023; published 14 July 2023)

The decay properties of ^{133}In were studied in detail at the ISOLDE Decay Station. The implementation of the Resonance Ionization Laser Ion Source allowed separate measurements of its $9/2^+$ ground state (^{133g}In) and $1/2^-$ isomer (^{133m}In). With the use of β-delayed neutron and γ spectroscopy, the decay strengths above the neutron separation energy were quantified in this neutron-rich nucleus for the first time. The allowed Gamow-Teller transition $9/2^+ \rightarrow 7/2^+$ was located at 5.93 MeV in the ^{133g}In decay with a $\log ft = 4.7(1)$. In addition, several neutron-unbound states were populated at lower excitation energies by the first-forbidden decays of ^{133g,m}In. We assigned spins and parities to those neutron-unbound states based on the β-decay selection rules, the $\log ft$ values, and systematics.

DOI: 10.1103/PhysRevC.108.014314

I. INTRODUCTION

Doubly magic nuclei far from the stability line, such as ^{24}O, ^{78}Ni, ^{100}Sn, and ^{132}Sn, have attracted tremendous interest in the last decades. Their simple structures and imbalanced neutron-proton ratios provide a testing ground to study the nuclear shell evolution as a function of isospin both

experimentally and theoretically; see, for example, Refs. [1–5] and references therein. It has been suggested that the residual nucleon-nucleon interactions are responsible for the drift of single-particle orbitals and the modification of nuclear shell structure at extreme neutron-proton ratios [6]. Since these phenomena impact the decay properties of nuclei, nuclear β decay is a viable probe to study the shell evolution. Specifically, nuclear β decay is extremely sensitive to the occupation of proton and neutron orbitals. In the neutron-rich nuclei, the predominant allowed Gamow-Teller (GT) transitions require $\Delta L = 0$ (L refers to the orbital angular momentum of proton and neutron) between neutron and proton spin-orbital partners in the same shell. The first-forbidden (FF) transitions, on the other hand, connect neutron and proton orbitals with $\Delta L = 1$ from neighboring shells. Due to their different selection rules, the GT and FF operators transform the initial state of the parent nucleus into diverse groups of final states in the daughter. Thus, measuring the decay strengths as a function of excitation energy provides nuclear-structure information in the parent and daughter nuclei. In addition, β decays play an important role in various nucleosynthesis processes. In the r process, for example, they compete with the rapid neutron-capture reaction and affect the final elemental distribution [7,8]. Owing to these reasons, it is of particular interest to measure the β-decay properties in the vicinity of ^{132}Sn. Its proton and neutron shell closures at $Z = 50$ and $N = 82$ define one of the strongest doubly magic cores on the neutron-rich side of the nuclear chart [4,9,10], providing a reference point to study nuclear structure with extreme neutron excess. Furthermore, the proximity of the r-process path to ^{132}Sn gives those decay properties key impacts on the r-process abundance pattern near the mass number $A = 130$ region [11].

In this work, we studied the β decay of ^{133}In, a nucleus southeast of ^{132}Sn. Because of its substantial Q_β window ($\approx$13 MeV), a large number of states with different microscopic configurations can be populated in the daughter ^{133}Sn. The states below the neutron separation energy were attributed to a single neutron outside the ^{132}Sn core [4,12,13]. The decay channels feeding those states can be understood by transforming a neutron above $N = 82$ into a proton below $Z = 50$ (e.g., $\nu f_{7/2} \rightarrow \pi g_{9/2}$). The subsequent γ decays had been surveyed thoroughly by Piersa *et al.* and Benito *et al.* [14,15]. The current study focused on the measurement of decay strength above the neutron separation energy, which was less known experimentally. The investigated states were highly excited because they were dominated by the neutron or proton particle-hole (p-h) excitations with respect to the ^{132}Sn core. Promptly after the β decays, neutrons were emitted from those states, leaving the residual ^{132}Sn in either the ground state or excited states. Some of the experimental findings and their consequences were highlighted in Ref. [16]. This article explains in full detail the experimental setup (Sec. II), the procedure to reconstruct the excitation energies of the neutron-unbound states and their β-decay feeding probabilities (Sec. III), and the spin-parity assignments of these states (Sec. IV).

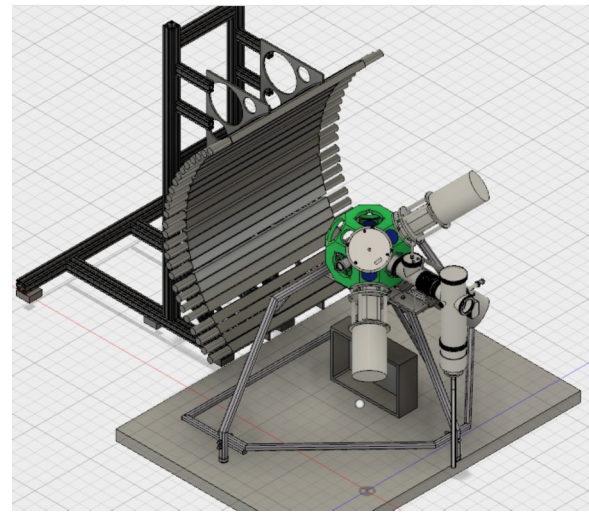

FIG. 1. Schematic drawing of experimental setup at IDS. The radioactive beam from ISOLDE was implanted on the tape at the center of the setup. The β-delayed γ rays from ^{133}In were detected by four HPGe clover detectors at backward angles relative to the beam direction. The INDiE array was placed on the other side to measure neutron spectroscopy following the ^{133}In decay.

II. EXPERIMENT

The neutron-rich indium isotopes were produced at the Isotope Separator On-Line (ISOLDE) facility at CERN [17]. A 1.4-GeV proton beam was delivered by the Proton Synchrotron Booster (PSB) and impinged on a tungsten solid neutron converter [18] with an average current of 2 μA. Radioactive isotopes, including ^{133}In, were produced in a uranium carbide (UC_x) target next to the neutron converter through neutron-induced fission. The indium atoms were ionized using the Resonance Ionization Laser Ion Source (RILIS) at ISOLDE [19]. By using the narrow-band titanium-sapphire (Ti:Sa) laser at RILIS [20], selective ionization of ^{133}In of either the ground state or isomer can be achieved [14]. Following the General Purpose Separator (GPS) [17] separating the isotopes of interest based on the mass-to-charge ratio, electrostatic dipoles and quadrupoles transported the ion beam to the ISOLDE Decay Station (IDS). The beam was implanted into a movable tape at the center of a decay chamber. After each proton pulse, the beam gate at ISOLDE was switched on for 300 ms for continuous implantation. Then, the implantation was stopped for 300 ms before the tape was rolled down to a shielded box to remove long-lived activities originating from the daughter and granddaughter β decays. The implantation and tape move cycle provided a 600-ms time window to measure decay products from the implanted ^{133}In.

Figure 1 draws the detector configuration at IDS. Four high-purity germanium (HPGe) clover detectors were placed closely outside the decay chamber to measure β-delayed γ radiation. The photopeak efficiency was 10% and 4% for 100-keV and 1-MeV γ rays, respectively, including combining energy deposition from Compton scattering inside all four crystals in each clover (addback). The neutron energies

E_n were deduced from their time-of-flight (TOF) measured by the IDS Neutron Detector (INDiE), an array similar to the Versatile Array of Neutron Detectors at Low Energy (VANDLE) [21,22]. The detection setup consisted of 26 EJ-200 plastic scintillator modules. Each module was $3 \times 6 \times 120$ cm^3 and had one photomultiplier tube (PMT) coupled to each end. The modules were mounted in a custom-built support frame describing an arch for a radius of 100 cm from the decay chamber. The intrinsic neutron efficiency of each module was 55% at 1 MeV [21]. The total solid angle covered by 26 modules was about 11.7% of 4π. However, only 22 out of 26 modules were used in the analysis due to the shadow from the supporting frame of the decay chamber. The resulting solid angle was 10.0% of 4π. Two plastic scintillators surrounding the implantation tape defined the start signal of TOF. They provided average efficiency of up to $\approx$80% for β particles. The neutron data were taken in the so-called triple coincidence mode, requiring both PMTs of an INDiE module and one of the β triggers to record an event. This way, the neutron detection threshold was pushed down to 100 keV (or 5-keV$_{ee}$ energy loss in the detectors). The traces of β and INDiE signals were sampled by the 12-bit 250-MHz digitizers. The subnanosecond time resolution was achieved using the algorithm introduced in Ref. [23]. The FWHM of the γ-flash peak in the obtained TOF spectrum was 1.5 ns. The actual neutron TOF distance between the implantation point and INDiE modules was determined as 104.2(3) cm using the online β decay of ^{17}N, which emits three fully resolved and well-studied neutron lines [24].

III. ANALYSIS OF THE NEUTRON SPECTRUM

Figures 2(a)–2(g) present the neutron data taken in coincidence with the β decay of ^{133}In. The figures on the left [Figs. 2(a)–2(d)] are taken with the ^{133g}In decay and those on the right [Figs. 2(e)–2(g)] with an admixture of ^{133g}In (40%) and ^{133m}In decays (60%). When RILIS was set on the $1/2^-$ isomer, there are still ^{133g}In implanted into the decay station at the same time, giving rise to the contamination peaks in the isomer's neutron spectra.

Figures 2(a) and 2(e) show the collected neutron spectra in two-dimensional (2D) histograms plotting the neutron TOF versus their energy loss in INDiE. The neutron events are seen following the banana-shaped distribution in the histograms. The neutron TOF spectra in Figs. 2(b) and 2(f) were made by projecting the 2D histograms along the x axis with energy loss greater than 5 keV$_{ee}$. Due to the simple structure of ^{133}Sn and the β-decay selection rules, only a few prominent neutron peaks were visible in the spectra. Furthermore, no major peaks were observed in coincidence with γ decays in ^{132}Sn, including the strongest $2^+_1 \rightarrow 0^+_{\text{g.s.}}$ transition, see Fig. 2(c). This implied those ^{133}Sn unbound states had a direct feeding to the ^{132}Sn ground state via neutron emissions. This lack of neutron-γ cascades was due to the first-excited state (2^+) in ^{132}Sn being above 4 MeV, making it energetically impossible for most of the neutron unbound states observed in the ^{133}In decay. Nevertheless, there was a small number of neutron emissions populating the ^{132}Sn excited states. Their numbers were estimated from the TOF spectra gated by the 4041-, 4352-, and 4416-keV γ rays observed by the clover detectors. These γ rays correspond to the $2^+_1 \rightarrow 0^+_{\text{g.s.}}$, $3^-_1 \rightarrow 0^+_{\text{g.s.}}$, and $4^+_1 \rightarrow 0^+_{\text{g.s.}}$ transitions in ^{132}Sn, respectively. According to Ref. [15], they carry mostly the entire γ-decay strength, via γ-γ cascade, from an excited state to the ground state, with a 5131-keV state being the sole exception. However, Ref. [15] reported an extremely weak ground-state-feeding branching ratio from this state. Thus, the error introduced by not considering this weak neutron-γ cascade was much smaller than the statistical uncertainties in the analysis. The result showed about 7.0(5)% of total neutron emissions going to the ^{132}Sn excited states. Their contribution was subtracted from the total neutron activity to ensure the neutron intensities feeding the ground state were extracted properly.

The neutron TOF spectra in Figs. 2(b) and 2(f) were fit by a template neutron response function. The procedure to determine the response function of individual peaks is explained as follows: First, the TOF spectrum was simulated for monoenergetic neutrons with GEANT4 [25], which took into account all the neutron-scattering material at IDS and the time resolution of INDiE modules. Second, the simulated profile was convolved with a Breit-Wigner style distribution [26] if a state had a sizable width in energy (broad resonance) greater than our resolution. The obtained response function was verified using the β decays of ^{49}K and ^{17}N, reproducing their neutron spectra with only known peaks from the literature [24,27]. Fitting the spectra of the ^{133}In decays only involved "zero-width" peaks in the response function. This indicated the observed resonances in ^{133}Sn were narrower than our energy resolution, which was about 80 and 250 keV for 1- and 3-MeV neutrons, respectively, at the minimum-energy threshold (5 keV$_{ee}$). Since the contribution from neutron-γ cascades had been subtracted from the fit, the peak intensity in the response function gave access to the neutron intensities directly feeding the ^{132}Sn ground state. The experimental background, which was drawn as the dashed lines in Fig. 2, consisted of a double-exponential decaying tail from fast β-decay electrons and a constant plateau from random γ rays.

The results from a χ^2-fitting analysis in Figs. 2(b) and 2(f) are summarized in Table I and Fig. 3. The numbers of peaks in the response function to fit the ground-state and isomeric decays were 19 and 13, respectively. All the ground-state peaks were included in the analysis of isomeric decay due to contamination. Their contributions, as illustrated by the blue peaks in Fig. 2(f) [and Fig. 2(g)], were determined by fixing their relative intensities to the strongest peak at 41 ns with the ratios obtained from the ground-state decay. The neutron peaks associated with the isomeric decay were drawn in red in Fig. 2(f) [and Fig. 2(g)] to be differentiated from the ground-state peaks. The excitation energies E_{ex} were derived by summing the neutron kinetic energy, corrected by recoil energy, with the neutron separation energy $S_n = 2.399(3)$ MeV in ^{133}Sn [28]. The experimental error combined the uncertainty in neutron TOF centroid, flight distance, and neutron separation energy. In this analysis, the number of detected β decays N_β was determined from the number of detected neutrons divided by the β-delayed neutron emission probability (P_n), which is 90(3)% and 93(3)% for ^{133g}In and ^{133m}In,

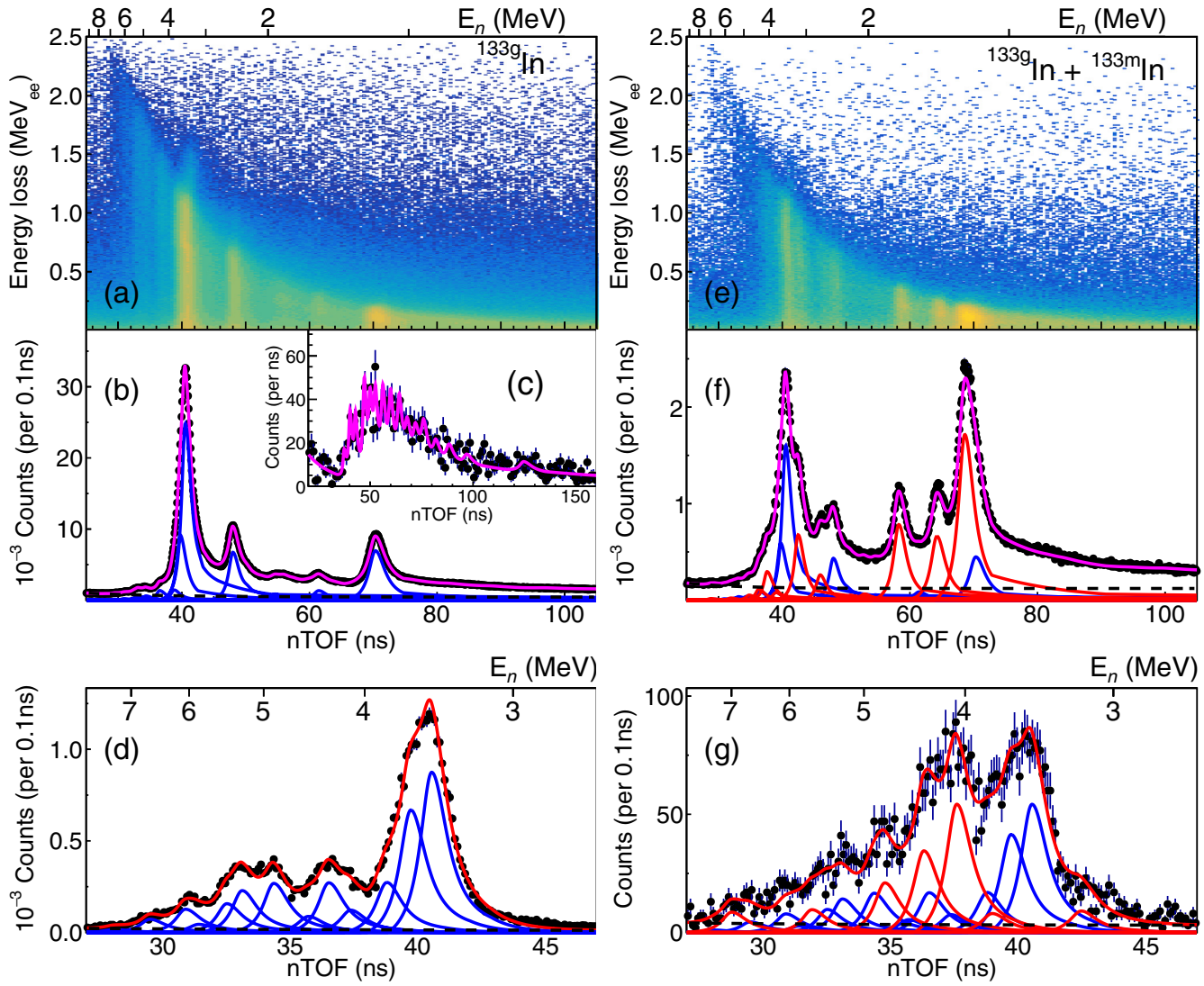

FIG. 2. The neutron data taken in coincidence with the ^{133}In β decay, with figures on the left corresponding to the pure ground-state decay and those on the right to an admixture of ground-state (40%) and isomeric decays (60%). Panels (a) and (e) plot the neutron TOF against their energy loss in INDiE, with the projections along TOF in panels (b) and (f), respectively. Panel (c) shows the ground-state neutron spectrum in coincidence with the 4041-keV γ decay in ^{132}Sn. Panels (d) and (g) focus on the TOF of high-energy neutrons with $E_n > 3$ MeV. They were made by projecting panels (a) and (e), respectively, along TOF with energy loss greater than 1 MeV$_{ee}$. All the neutron TOF spectra were fit by the neutron response functions (magenta), with the neutron peaks attributed to the ground-state and isomeric decays drawn in blue and red, respectively. The dashed line is the β- and γ-ray background in the neutron TOF spectra.

respectively [15]. Then, the decay probability I_β of the state was calculated by normalizing the neutron intensity to N_β. In cases where there were γ decays competing with neutron emissions, which will be discussed in more detail later, I_β included the contribution from γ decays. Note that all I_β in Table I were calculated from the neutron emissions directly feeding the ^{132}Sn ground state. It is strictly correct for the states below 6.44 MeV in ^{133}Sn. For the states above 6.44 MeV, where the neutron-γ cascade is energetically possible, these I_β should be regarded as the lower limits. The ground-state (isomeric) decay logft values were extracted using the I_β in Table I, the β-decay half-life of ^{133g}In (^{133m}In) from Ref. [14], and the $Q_\beta = 13.2$ MeV (13.8 MeV) from the atomic mass difference between ^{133g}In (^{133m}In) [29] and ^{133}Sn [28].

A high-energy part of the neutron spectra in Figs. 2(b) and 2(f), i.e., $E_n > 4$ MeV and TOF < 40 ns, is more likely due to a continuum of strength distribution rather than due to isolated resonances. There, a peak in the response function should be regarded as a neutron quasiresonance [22]. The distribution of transitions in the continuum was inferred by increasing the energy threshold of INDiE, resulting in better resolving power in the TOF spectrum than the previously quoted values. For instance, Figs. 2(d) and 2(g) present the spectra with 1-MeV$_{ee}$ energy threshold for the ^{133g,m}In decays, respectively, showing better resolution for the high-energy neutron peaks than Figs. 2(b) and 2(f). The centroids of the high-energy neutron peaks were determined in Figs. 2(d) and 2(g) before they were fixed in the fit of Figs. 2(b)

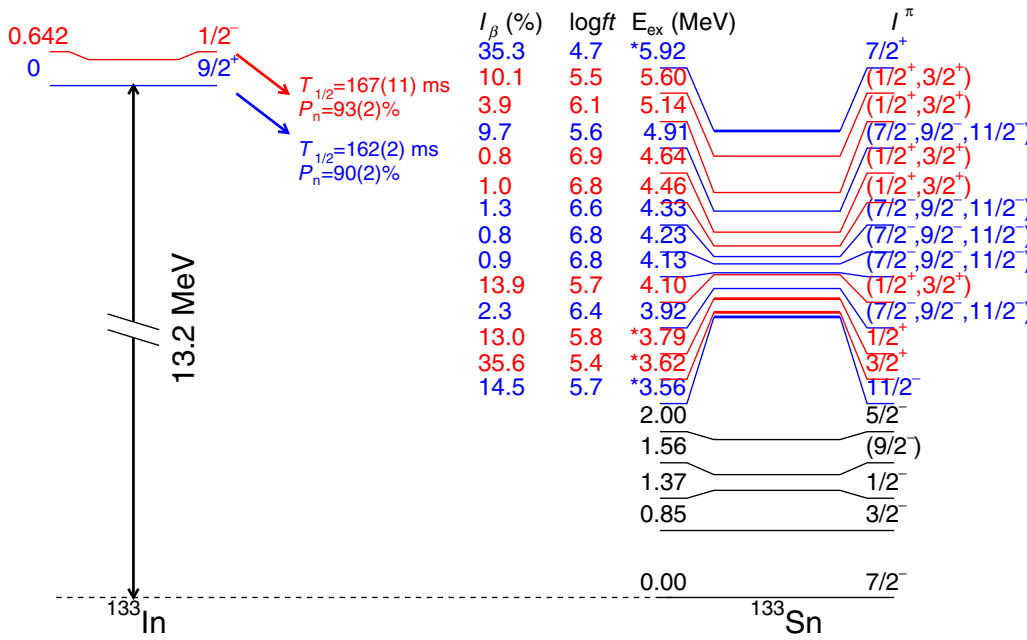

FIG. 3. Constructed decay schemes of ^{133g}In $(9/2^+)$ and ^{133m}In $(1/2^-)$ between $S_n = 2.399$ MeV [28] and $E_{ex} = 6.0$ MeV, where isolated resonances were observed in ^{133}Sn. Decays associated with the ground state and isomer are differentiated in blue and red, respectively. The states below the neutron separation energy are included for completeness [13,14]. Half-lives and neutron-emission probabilities (P_n) in ^{133}In are taken from Refs. [14,15]. The excitation energy of the $1/2^-$ isomer is from Ref. [29]. The states with a solid spin-parity assignment are highlighted by "$*$" on their excitation energies.

and 2(f) to extract intensities together with lower-energy neutron peaks.

The observations of γ decay from neutron-unbound states were reported previously in ^{133}Sn [14,15,30]. Therefore, both γ and neutron intensities were measured in this work to ensure no strength was missing in I_β. In the ^{133g}In decay, five γ peaks at 3564, 3928, 4110, 6018, and 6088 keV were found to have half-lives and energies consistent with the corresponding neutron peaks in Table I. These observed γ rays agree with the previous β-decay study of ^{133}In using pure γ-ray spectroscopy [14,15]. Figure 4 shows portions of γ-ray spectra in the relevant energy ranges. Statistically, none of these γ transitions were in coincidence with any other γ rays nor neutron emissions, suggesting they were single-γ transitions from a

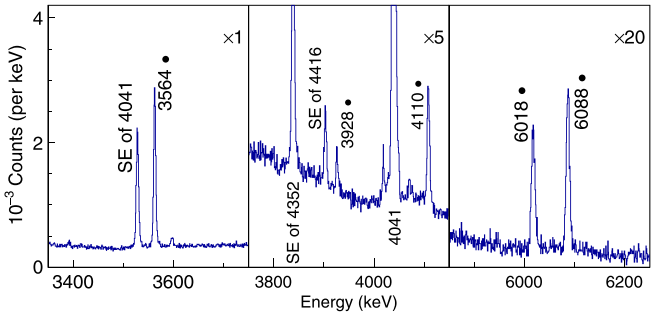

FIG. 4. Portion of γ-ray spectra measured in coincidence with the ground-state decay of ^{133}In. The candidate γ deexcitations from the ^{133}Sn neutron-unbound states are marked by "•," to be distinguished from the γ decays in ^{132}Sn. SE stands for "single-escape" peak. See text for details.

neutron unbound state to the ground state. For the transitions at 3564, 3928, and 4110 keV, their γ intensities were added to the I_β of 3562-, 3923-, and 4134-keV states in Table I, respectively. Regarding the two γ transitions around 6 MeV, their separation is only 70 keV, too close to be resolved by our neutron detectors. Instead, a neutron peak was observed at $E_n = 3642$ keV ($E_{ex} = 6068$ keV) with TOF ≈ 39.5 ns, see Fig. 2(d). Thus, it was presumed that the neutron peak consists of an unresolved doublet at 6018 and 6088 keV, respectively. The I_β of the 6068-keV state corresponds to the sum of the doublet. In contrast, no neutron-γ competition was identified following the ^{133m}In decay. Below 6-MeV excitation energy, where β feedings are strong, the $1/2^-$ isomer is expected to populate low-spin positive-parity states in ^{133}Sn via FF transitions. From those states, the electromagnetic (EM) $E2/M1$ transitions to the $7/2^-$ ground state in ^{133}Sn are forbidden, and higher-order EM transitions ($M2/E3$) are too slow to compete with neutron emissions. From a low-spin negative-parity state fed by GT transitions at higher energy, the neutron-γ competition is in principle possible, similar to ^{133g}In as discussed above. However, no such candidates were found due to the combined effect of smaller β feeding and a limited number of implanted samples.

Figure 5 presents the extracted β-strength distribution, in the form of $S_\beta = 1/ft$ [31], of the ^{133g,m}In decays with an energy interval of 200 keV. The distributions include the states listed in Table I and the decay strengths associated with the neutron emissions feeding the ^{132}Sn excited states, which is around 7% of total neutron emissions as discussed above. For these minor strengths, the neutron-γ coincidence analysis was needed to correct the excitation energies of the

TABLE I. A list of neutron-unbound states identified in ^{133}Sn. Those were derived from the neutron emissions directly feeding the ^{132}Sn ground state. The excitation energies E_{ex} were calculated from neutron TOF and the $S_n = 2.399(3)$ MeV [28]. The I_β is the β-decay-feeding probability given in % per β decay. A value with $*$ means the state decayed via competing neutron and γ channels, whereas that with † is likely a doublet at 6018 and 6088 keV, respectively. See text for details. The logft values were calculated using the half-lives from Ref. [14], β-decay Q_β from the atomic mass difference between ^{133}In [29] and ^{133}Sn [28], and E_{ex}, I_β from this work. Spins and parities I^π were assigned tentatively based on the β-decay selection rules, logft, and systematics.

Parent	E_{ex} (keV)	I^π	I_β (%)	logft
^{133g}In	3562(18)	$(11/2^-)$	14.5(8)*	5.7(1)
	3924(27)	$(7/2^-$–$11/2^-)$	2.3(1)*	6.4(1)
	4134(34)	$(7/2^-$–$11/2^-)$	0.9(1)*	6.8(1)
	4234(36)	$(7/2^-$–$11/2^-)$	0.8(1)	6.8(1)
	4334(38)	$(7/2^-$–$11/2^-)$	1.3(1)	6.6(1)
	4906(55)	$(7/2^-$–$11/2^-)$	9.7(3)	5.6(1)
	5925(91)	$(7/2^+)$	35.3(13)	4.7(1)
	6068(96)	(7/2–11/2)	13.6(7)†	5.1(1)
	6250(100)	(7/2–11/2)	2.0(2)	5.9(1)
	6550(120)	(7/2–11/2)	0.3(1)	6.6(1)
	6750(120)	(7/2–11/2)	2.1(1)	5.7(1)
	6950(130)	(7/2–11/2)	0.3(1)	6.6(1)
	7320(150)	(7/2–11/2)	1.1(1)	5.8(2)
	7700(160)	(7/2–11/2)	1.1(1)	5.7(2)
	7900(170)	(7/2–11/2)	0.7(1)	5.9(2)
	8300(190)	(7/2–11/2)	0.2(1)	6.3(2)
	8500(200)	(7/2–11/2)	0.5(1)	5.7(2)
	9100(230)	(7/2–11/2)	0.4(1)	5.6(2)
	9800(270)	(7/2–11/2)	0.1(1)	5.8(2)
^{133m}In	3621(19)	$(3/2^+)$	35.6(14)	5.4(1)
	3794(23)	$(1/2^+)$	13.0(5)	5.8(1)
	4096(30)	$(1/2^+, 3/2^+)$	13.9(5)	5.7(1)
	4460(44)	$(1/2^+, 3/2^+)$	1.0(2)	6.8(1)
	4638(49)	$(1/2^+, 3/2^+)$	0.8(2)	6.9(1)
	5137(62)	$(1/2^+, 3/2^+)$	3.9(2)	6.1(1)
	5604(78)	$(1/2^+, 3/2^+)$	10.1(5)	5.5(1)
	6210(100)	(1/2, 3/2)	1.3(3)	6.3(1)
	6500(110)	(1/2, 3/2)	5.0(4)	5.6(1)
	6800(120)	(1/2, 3/2)	2.1(2)	5.9(1)
	7200(140)	(1/2, 3/2)	1.1(2)	6.1(1)
	8110(180)	(1/2, 3/2)	0.6(2)	6.1(1)
	9450(250)	(1/2, 3/2)	0.6(2)	5.6(1)

neutron-unbound states in ^{133}Sn. This can be easily applied to the neutron emissions that feed the 2^+, 3^-, or 4^+ states in ^{132}Sn due to their relatively strong neutron-γ cascades. Additionally, Piersa *et al.* and Benito *et al.* observed weak neutron emissions feeding the states higher than the 4^+ state in ^{132}Sn [14,15]. Their observations were confirmed in our measurement, but the associated γ decays were generally too weak to perform credible neutron-γ coincidence analysis for the energy correction. To simplify the analysis and include their contribution in Fig. 5, two extreme cases were considered. First, the strength distribution was calculated assuming those weak neutron emissions only fed the lowest 2^+, 3^-, or 4^+ states around 4 MeV in ^{132}Sn. Second, the calculation was repeated with the ^{132}Sn state shifted to 6.5 MeV, the highest observed state in the β-delayed neutron emissions of ^{133g,m}In [15]. The final results shown in Fig. 5 are the average between the two calculations, with the error bars covering their upper and lower limits.

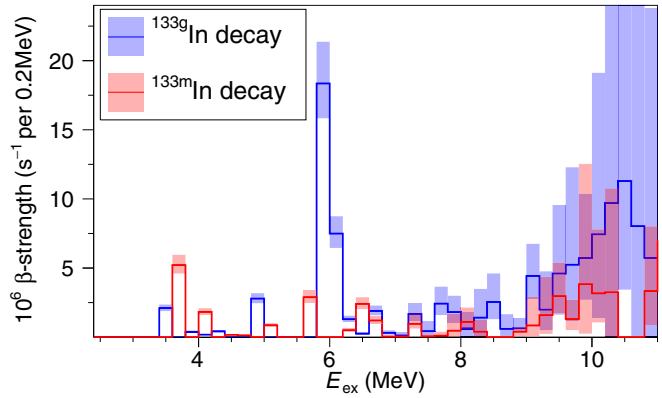

FIG. 5. The experimental β-decay strength distribution (in $S_\beta = 1/ft$ [31]) of the ^{133}In ground state (blue) and isomer (red) between $E_{ex} = 2.5$ and 11 MeV.

IV. SPIN AND PARITY ASSIGNMENTS

Before this work, the only state known to have a neutron-hole configuration in ^{133}Sn was the $11/2^-$ state at 3564 keV [12,14,30]. Its wave function is dominated by a neutron 2p-1h configuration, in which a neutron hole at $h_{11/2}$ couples to two neutron particles above $N = 82$. In the ^{133g}In decay, the same state was observed at $E_{ex} = 3562(18)$ keV, in good agreement with the literature value. It is the lowest neutron unbound state seen in the experiment (see Fig. 3). In an intuitive picture, the decay is associated with a FF transition $\nu h_{11/2} \rightarrow \pi g_{9/2}$, during which the two neutron particles outside $N = 82$ persist as a spin $J = 0$ pair in the initial and final states. Fogelberg *et al.* observed the analogous transition without the neutron pair in ^{131}In $\rightarrow$ ^{131}Sn with a log$ft > 5.6$ [32]. According to the odd-mass tin isotopes with $N < 82$, there are two extra neutron orbitals $d_{3/2}$ and $s_{1/2}$ close to $h_{11/2}$, giving rise to three neutron 2p-1h states at similar excitation energy in ^{133}Sn. Indeed, two states were observed in the isomeric decay at excitation energies of 3.62 and 3.79 MeV. Following the systematics, the lower state (logft = 5.4) was assigned $I^\pi = 3/2^+$, and the upper state (logft = 5.8) $I^\pi = 1/2^+$. Their underlying transitions are $\nu d_{3/2} \rightarrow \pi p_{1/2}$ and $\nu s_{1/2} \rightarrow \pi p_{1/2}$, respectively, both of which are FF transitions. The most important neutron-hole orbital involved in the ^{133}In decay is the deeply bound $\nu g_{7/2}$ because it determines the GT strength of ^{133g}In. In Fig. 5, one can see a remarkable strength at $E_{ex} = 5.93$ MeV exclusive to the ^{133g}In decay. Its I_β gives a log$ft = 4.7$, which is significantly stronger than any other feeding in the decay. Thus, the state was assigned $I^\pi = 7/2^+$ originating from $\nu g_{7/2}^{-1}$. The newly determined GT strength of $\nu g_{7/2} \rightarrow \pi g_{9/2}$ in ^{133g}In has a similar logft as in the ^{131g}In decay (=4.4 [32]). Note that this

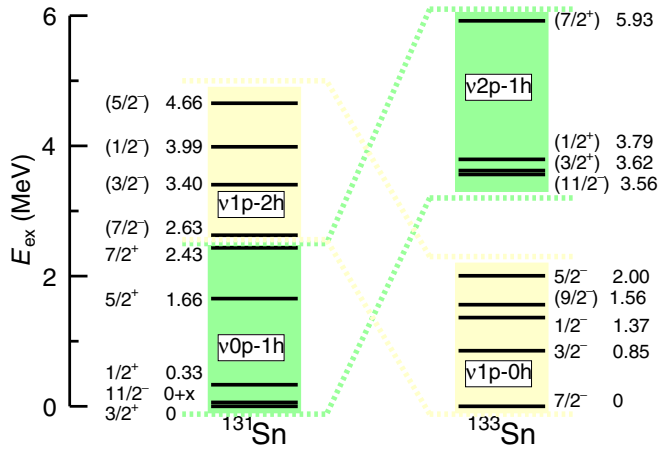

FIG. 6. Reduced level schemes of ^{131}Sn and ^{133}Sn. Each group of states is labeled by the dominant neutron p-h configuration in the wave functions. Information in ^{131}Sn is taken from Refs. [32,33]. In ^{133}Sn, the spins, parities, and excitation energies of the ν1p-0h states are taken from Refs. [13,14], while those of ν2p-1h are from this work. The dashed lines connect groups of states with the same odd-even combination of neutron p-h configuration.

assignment is different from that in Ref. [14] suggesting the 6088-keV state to be populated via the dominant GT decay.

The result enables a complete comparison between ^{131}Sn and ^{133}Sn, see Fig. 6. Before this work, the neutron 1p-2h states in ^{131}Sn and the neutron 1p-0h states in ^{133}Sn had revealed remarkable similarity in neutron transfer reactions [4,33]. Similarly, if one moved down the neutron 2p-1h states in ^{133}Sn and aligned the lowest $11/2^-$ state to the ground state in ^{131}Sn, the level scheme constructed in this work is analogous to that of the 0p-1h states in ^{131}Sn [32], supporting our spin-parity assignment discussed previously.

Besides, one notices strong β feedings at $E_{ex} \approx 5$ MeV in Fig. 5 in both ground-state and isomeric decays. At this excitation energy, it is possible to break the proton $Z = 50$ core and populate the proton 1p-1h excited states in ^{133}Sn. From the low-lying states in odd-mass antimony isotopes ($Z = 51$) around $N = 82$, $\pi g_{7/2}$ and $\pi d_{5/2}$ are expected to be the lowest two-proton orbitals outside $Z = 50$. Thus, the lowest proton core excited states observed in the ^{133}In decay should be dominated by either $\pi(g_{9/2}^{-1}\ g_{7/2}) \times \nu f_{7/2}$ or $\pi(p_{1/2}^{-1}\ g_{7/2}) \times \nu f_{7/2}$, depending on where the proton hole is in the initial state, i.e., whether the ground-state or isomeric decay. Both scenarios are carried by the FF transition $\nu f_{7/2} \rightarrow \pi g_{7/2}$. At slightly higher excitation energy, states with the $\pi(g_{9/2}^{-1}\ d_{5/2}) \times \nu f_{7/2}$ or $\pi(p_{1/2}^{-1}\ d_{5/2}) \times \nu f_{7/2}$ configuration should also be accessible via $\nu f_{7/2} \rightarrow \pi d_{5/2}$. Benito *et al.* observed analogous transitions in the decay from ^{132}In to ^{132}Sn at similar excitation energy [15]. The I^π of those states were assigned based on the β-decay selection rules of nonunique FF transitions: $\Delta I = 0$ or 1 and $\Delta\pi = -1$. The unique FF transitions with $\Delta I = 2$ were not considered in the present spin assignment due to their significantly larger $\log ft$ and smaller intensities [34]. For example, the neutron $d_{5/2}^{-1}$ state in ^{131}Sn is populated in the isomeric decay of ^{131}In ($\nu d_{5/2} \rightarrow \pi p_{1/2}$) with a $\log ft = 9.5$ [32], of which the feeding probability is far below our sensitivity.

Above the $7/2^+$ state at 5.93 MeV, no isolated resonances were seen with strong feeding strength in either of the ^{133g,m}In decay. The spectra follow a continuous distribution, which was attributed to the high level density and limited resolving power. In this energy region, β decay can populate both positive- and negative-parity states via GT or FF transitions. The GT transitions are favored because of their more significant matrix elements. Following the selection rule, the states with $E_{ex} > 6$ MeV were assigned the spin $I = (7/2,\ 9/2,\ 11/2)$ in the ground-state decay and $(1/2,\ 3/2)$ in the isomeric decay.

V. SUMMARY AND CONCLUSIONS

In this work, the β-decay properties of ^{133g,m}In were studied at IDS. With the use of β-delayed γ and neutron spectroscopy, their major components in the decay-strength distribution were located above the neutron separation energy in the daughter ^{133}Sn. The strong GT transformation $\nu g_{7/2} \rightarrow \pi g_{9/2}$ was observed in the ^{133g}In decay, feeding a $7/2^+$ state at 5.93 MeV in ^{133}Sn. Besides, many neutron-unbound states originating from neutron or proton p-h excitations were found at lower energies following the FF decays of ^{133g,m}In. The spins and parities of those states were assigned tentatively based on the β-decay selection rules, the extracted $\log ft$ values, and systematics along the isotopic chain.

The experimental findings greatly extend our knowledge of the ^{133}In decay from previous works [12,14,15], providing the β-strength distribution southeast of ^{132}Sn. The results are crucial to benchmark β-decay theories and will serve as a bridge to understand the decay properties of more neutron-rich nuclei, e.g., those r-process waiting-point nuclei near the $N = 82$ shell closure.

ACKNOWLEDGMENTS

We acknowledge the support of the ISOLDE Collaboration and technical teams. This project was supported by the European Unions Horizon 2020 research and innovation programme Grant Agreements No. 654002 (ENSAR2) and the Marie Skłodowska-Curie Grant Agreement No. 101032999 (BeLaPEx), by the Office of Nuclear Physics, U.S. Department of Energy under Awards No. DE-FG02-96ER40983 (UTK) and No. DE-AC05-00OR22725 (ORNL), by the National Nuclear Security Administration under the Stewardship Science Academic Alliances program through DOE Award No. DE-NA0002132, by the Romanian IFA project CERN-RO/ISOLDE, by the Research Foundation Flanders (FWO, Belgium), by the Interuniversity Attraction Poles Programme initiated by the Belgian Science Policy Office (BriX network P7/12), by the German BMBF under Contracts No. 05P18PKCIA and No. 05P21PKCI1 in Verbundprojekte 05P2018 and 05P2021, by the UK Science and Technology Facilities Research Council (STFC) of the UK Grants No. ST/R004056/1, No. ST/P004598/1, No. ST/P003885/1, No. ST/V001027/1, and No. ST/V001035/1, by National Natural Science Foundation of China under Grant No. 11775316, by the Polish National Science Center under

Grant No. 2020/39/B/ST2/02346, by the Polish Ministry of Education and Science under Contract No. 2021/WK/07, by Spanish MCIN/AEI under Grants No. PGC2018-093636-B-I00, No. RTI2018-098868-B-I00, No. PID2019-104390GB-I00, No. PID2019-104714GB-C21, and No. PID2021-126998OB-I00, by Generalitat Valenciana, Conselleria de Innovación, Universidades, Ciencia y Sociedad Digital under Grant No. CISEJI/2022/25, by Universidad Complutense de Madrid (Spain) through Grupo de Física Nuclear under Grant No. 910059 and through the Predoctoral Grant No. CT27/16-CT28/16, and by the EU via NextGenerationEU funds.

[1] R. Kanungo, C. Nociforo, A. Prochazka, T. Aumann, D. Boutin, D. Cortina-Gil, B. Davids, M. Diakaki, F. Farinon, H. Geissel, R. Gernhäuser, J. Gerl, R. Janik, B. Jonson, B. Kindler, R. Knöbel, R. Krücken, M. Lantz, H. Lenske, Y. Litvinov *et al.*, Phys. Rev. Lett. **102**, 152501 (2009).

[2] R. Taniuchi, C. Santamaria, P. Doornenbal, A. Obertelli, K. Yoneda, G. Authelet, H. Baba, D. Calvet, F. Château, A. Corsi, A. Delbart, J. M. Gheller, A. Gillibert, J. D. Holt, T. Isobe, V. Lapoux, M. Matsushita, J. Menéndez, S. Momiyama, T. Motobayashi *et al.*, Nature (London) **569**, 53 (2019).

[3] C. B. Hinke, M. Böhmer, P. Boutachkov, T. Faestermann, H. Geissel, J. Gerl, R. Gernhäuser, M. Górska, A. Gottardo, H. Grawe, J. L. Grębosz, R. Krücken, N. Kurz, Z. Liu, L. Maier, F. Nowacki, S. Pietri, Z. Podolyák, K. Sieja, K. Steiger *et al.*, Nature (London) **486**, 341 (2012).

[4] K. L. Jones, A. S. Adekola, D. W. Bardayan, J. C. Blackmon, K. Y. Chae, K. A. Chipps, J. A. Cizewski, L. Erikson, C. Harlin, R. Hatarik, R. Kapler, R. L. Kozub, J. F. Liang, R. Livesay, Z. Ma, B. H. Moazen, C. D. Nesaraja, F. M. Nunes, S. D. Pain, N. P. Patterson *et al.*, Nature (London) **465**, 454 (2010).

[5] A. R. Vernon, R. F. Garcia Ruiz, T. Miyagi, C. L. Binnersley, J. Billowes, M. L. Bissell, J. Bonnard, T. E. Cocolios, J. Dobaczewski, G. J. Farooq-Smith, K. T. Flanagan, G. Georgiev, W. Gins, R. P. de Groote, R. Heinke, J. D. Holt, J. Hustings, Á. Koszorús, D. Leimbach, K. M. Lynch *et al.*, Nature (London) **607**, 260 (2022).

[6] O. Sorlin and M.-G. Porquet, Prog. Part. Nucl. Phys. **61**, 602 (2008).

[7] E. M. Burbidge, G. R. Burbidge, W. A. Fowler, and F. Hoyle, Rev. Mod. Phys. **29**, 547 (1957).

[8] A. G. Cameron, *Stellar Evolution, Nuclear Astrophysics, and Nucleogenesis*, Technical Report, 2nd edition (Atomic Energy of Canada Ltd, Chalk River, Ontario, 1957), Vol. CRL-41.

[9] A. Kerek, G. Holm, L.-E. De Geer, and S. Borg, Phys. Lett. B **44**, 252 (1973).

[10] T. Björnstad, M. Borge, J. Blomqvist, R. Von Dincklage, G. Ewan, P. Hoff, B. Jonson, K. Kawade, A. Kerek, O. Klepper, G. Lövhöiden, S. Mattsson, G. Nyman, H. Ravn, G. Rudstam, K. Sistemich, and O. Tengblad, Nucl. Phys. A **453**, 463 (1986).

[11] M. Mumpower, R. Surman, G. McLaughlin, and A. Aprahamian, Prog. Part. Nucl. Phys. **86**, 86 (2016).

[12] P. Hoff, P. Baumann, A. Huck, A. Knipper, G. Walter, G. Marguier, B. Fogelberg, A. Lindroth, H. Mach, M. Sanchez-Vega, R. B. E. Taylor, P. Van Duppen, A. Jokinen, M. Lindroos, M. Ramdhane, W. Kurcewicz, B. Jonson, G. Nyman, Y. Jading, K.-L. Kratz, A. Wöhr, G. Løvhøiden, T. F. Thorsteinsen, and J. Blomqvist (ISOLDE Collaboration), Phys. Rev. Lett. **77**, 1020 (1996).

[13] J. M. Allmond, A. E. Stuchbery, J. R. Beene, A. Galindo-Uribarri, J. F. Liang, E. Padilla-Rodal, D. C. Radford, R. L. Varner, A. Ayres, J. C. Batchelder, A. Bey, C. R. Bingham, M. E. Howard, K. L. Jones, B. Manning, P. E. Mueller, C. D. Nesaraja, S. D. Pain, W. A. Peters, A. Ratkiewicz *et al.*, Phys. Rev. Lett. **112**, 172701 (2014).

[14] M. Piersa, A. Korgul, L. M. Fraile, J. Benito, E. Adamska, A. N. Andreyev, R. Álvarez-Rodríguez, A. E. Barzakh, G. Benzoni, T. Berry, M. J. G. Borge, M. Carmona, K. Chrysalidis, J. G. Correia, C. Costache, J. G. Cubiss, T. Day Goodacre, H. De Witte, D. V. Fedorov, V. N. Fedosseev *et al.* (IDS Collaboration), Phys. Rev. C **99**, 024304 (2019).

[15] J. Benito, L. M. Fraile, A. Korgul, M. Piersa, E. Adamska, A. N. Andreyev, R. Álvarez-Rodríguez, A. E. Barzakh, G. Benzoni, T. Berry, M. J. G. Borge, M. Carmona, K. Chrysalidis, C. Costache, J. G. Cubiss, T. Day Goodacre, H. De Witte, D. V. Fedorov, V. N. Fedosseev, G. Fernández-Martínez, and N. Warr (IDS Collaboration), Phys. Rev. C **102**, 014328 (2020).

[16] Z. Y. Xu *et al.*, Phys. Rev. Lett. **131**, 022501 (2023).

[17] R. Catherall, W. Andreazza, M. Breitenfeldt, A. Dorsival, G. J. Focker, T. P. Gharsa, G. T. J, J.-L. Grenard, F. Locci, P. Martins, S. Marzari, J. Schipper, A. Shornikov, and T. Stora, J. Phys. G **44**, 094002 (2017).

[18] A. Gottberg, T. Mendonca, R. Luis, J. Ramos, C. Seiffert, S. Cimmino, S. Marzari, B. Crepieux, V. Manea, R. Wolf, F. Wienholtz, S. Kreim, V. Fedosseev, B. Marsh, S. Rothe, P. Vaz, J. Marques, and T. Stora, Nucl. Instrum. Methods Phys. Res., Sect. B **336**, 143 (2014).

[19] V. Fedosseev, K. Chrysalidis, T. D. Goodacre, B. Marsh, S. Rothe, C. Seiffert, and K. Wendt, J. Phys. G **44**, 084006 (2017).

[20] S. Rothe, V. Fedosseev, T. Kron, B. Marsh, R. Rossel, and K. Wendt, Nucl. Instrum. Methods Phys. Res., Sect. B **317**, 561 (2013).

[21] W. Peters, S. Ilyushkin, M. Madurga, C. Matei, S. Paulauskas, R. Grzywacz, D. Bardayan, C. Brune, J. Allen, J. Allen, Z. Bergstrom, J. Blackmon, N. Brewer, J. Cizewski, P. Copp, M. Howard, R. Ikeyama, R. Kozub, B. Manning, T. Massey *et al.*, Nucl. Instrum. Methods Phys. Res., Sect. A **836**, 122 (2016).

[22] M. Madurga, S. V. Paulauskas, R. Grzywacz, D. Miller, D. W. Bardayan, J. C. Batchelder, N. T. Brewer, J. A. Cizewski, A. Fijałkowska, C. J. Gross, M. E. Howard, S. V. Ilyushkin, B. Manning, M. Matoš, A.J. Mendez, II, K. Miernik, S. W. Padgett, W. A. Peters, B. C. Rasco, A. Ratkiewicz *et al.*, Phys. Rev. Lett. **117**, 092502 (2016).

[23] S. Paulauskas, M. Madurga, R. Grzywacz, D. Miller, S. Padgett, and H. Tan, Nucl. Instrum. Methods Phys. Res., Sect. A **737**, 22 (2014).

[24] H. Ohm, W. Rudolph, and K.-L. Kratz, Nucl. Phys. A **274**, 45 (1976).

[25] S. Agostinelli, J. Allison, K. Amako, J. Apostolakis, H. Araujo, P. Arce, M. Asai, D. Axen, S. Banerjee, G. Barrand, F. Behner, L. Bellagamba, J. Boudreau, L. Broglia, A. Brunengo, H. Burkhardt, S. Chauvie, J. Chuma, R. Chytracek, G. Cooperman

et al., Nucl. Instrum. Methods Phys. Res., Sect. A **506**, 250 (2003).
[26] G. Nyman, R. Azuma, P. Hansen, B. Jonson, P. Larsson, S. Mattsson, A. Richter, K. Riisager, O. Tengblad, and K. Wilhelmsen, Nucl. Phys. A **510**, 189 (1990).
[27] L. Carraz, P. Hansen, A. Huck, B. Jonson, G. Klotz, A. Knipper, K. Kratz, C. Miéhé, S. Mattsson, G. Nyman, H. Ohm, A. Poskanzer, A. Poves, H. Ravn, C. Richard-Serre, A. Schröder, G. Walter, and W. Ziegert, Phys. Lett. B **109**, 419 (1982).
[28] M. Wang, W. Huang, F. Kondev, G. Audi, and S. Naimi, Chin. Phys. C **45**, 030003 (2021).
[29] C. Izzo, J. Bergmann, K. A. Dietrich, E. Dunling, D. Fusco, A. Jacobs, B. Kootte, G. Kripkó-Koncz, Y. Lan, E. Leistenschneider, E. M. Lykiardopoulou, I. Mukul, S. F. Paul, M. P. Reiter, J. L. Tracy, C. Andreoiu, T. Brunner, T. Dickel, J. Dilling, I. Dillmann *et al.*, Phys. Rev. C **103**, 025811 (2021).
[30] V. Vaquero, A. Jungclaus, P. Doornenbal, K. Wimmer, A. Gargano, J. A. Tostevin, S. Chen, E. Nácher, E. Sahin, Y. Shiga, D. Steppenbeck, R. Taniuchi, Z. Y. Xu, T. Ando, H. Baba, F. L. B. Garrote, S. Franchoo, K. Hadynska-Klek, A. Kusoglu, J. Liu *et al.*, Phys. Rev. Lett. **118**, 202502 (2017).
[31] C. Duke, P. Hansen, O. Nielsen, and G. Rudstam, Nucl. Phys. A **151**, 609 (1970).
[32] B. Fogelberg, H. Gausemel, K. A. Mezilev, P. Hoff, H. Mach, M. Sanchez-Vega, A. Lindroth, E. Ramström, J. Genevey, J. A. Pinston, and M. Rejmund, Phys. Rev. C **70**, 034312 (2004).
[33] R. L. Kozub, G. Arbanas, A. S. Adekola, D. W. Bardayan, J. C. Blackmon, K. Y. Chae, K. A. Chipps, J. A. Cizewski, L. Erikson, R. Hatarik, W. R. Hix, K. L. Jones, W. Krolas, J. F. Liang, Z. Ma, C. Matei, B. H. Moazen, C. D. Nesaraja, S. D. Pain, D. Shapira *et al.*, Phys. Rev. Lett. **109**, 172501 (2012).
[34] B. Singh, J. Rodriguez, S. Wong, and J. Tuli, Nucl. Data Sheets **84**, 487 (1998).